Chapter 5

Manganese Oxidation Induced by Water Table Fluctuations in a Sand Column

Abstract

On-off cycles of production wells, especially in bank filtration settings, cause oscillations in the local water table, which can deliver significant amounts of dissolved oxygen (DO) to the shallow groundwater. The potential for DO introduced in this manner to oxidize manganese (Mn), mediated by the obligate aerobe *Pseudomonas putida* GB-1, was tested in a column of quartz sand fed with anoxic influent solution and subject to 1.3 m water table changes every 30–50 h. After a period of filter ripening, 100 μM Mn was rapidly removed during periods of low water table and high dissolved oxygen concentrations. The accumulation of Mn in the column was confirmed by XRF analysis of the sand at the conclusion of the study, and both measured net oxidation rates and XAS analysis suggest microbial oxidation as the dominant process. The addition of Zn, which inhibited GB-1 Mn oxidation but not its growth, interrupted the Mn removal process, but Mn oxidation recovered within one water table fluctuation. Thus transient DO conditions could support Mn oxidation, and this process could be more relevant in shallow groundwater than previously thought.

Introduction

Groundwater extracted for drinking water often has manganese (Mn) and iron (Fe) concentrations above the WHO guidelines (Massmann et al. 2007, de Vet et al. 2010). Post-extraction treatment in aerated sand filters is effective in decreasing Mn and Fe concentrations (Mouchet 1992), but it is possible that well operation could promote *in situ* Mn and Fe removal. On-off cycles of production wells in bank filtration sites, for example, cause oscillations in the local water table (Massmann and Sültenfuß 2008). These fluctuations entrap air and deliver O_2 to the shallow groundwater (Beyerle et al. 1999, Williams and Oostrom 2000, Kohfahl et al. 2009).

Subsurface Fe removal exploits this process in (partly) controlled systems: O_2-saturated groundwater is injected into the subsurface to oxidize Fe. Resumption of groundwater extraction from the well leads to Fe(II) sorption to Fe(III) oxides, and upon breakthrough of Fe, another pulse of O_2-saturated groundwater is injected. Succeeding cycles lead to an expansion of the zone of Fe removal and increased efficiency in the process, with no significant clogging (Hallberg and Martinell 1976, Appelo et al. 1999, Mettler et al. 2001). It has been observed at some sites that subsurface Fe removal wells require less frequent rehabilitation than typical extraction-only groundwater wells (van Beek 1985, van Halem et al. 2011).

In comparison with Fe, the kinetics of Mn oxidation by O_2 are much slower and require microbial mediation at circumneutral pH (Morgan 2000, Tebo et al. 2004). The presence of dissolved Fe(II) also precludes significant Mn oxide accumulation, as Fe(II) rapidly reduces Mn oxides (Postma and Appelo 2000). Mn removal in subsurface Fe removal sites is limited (Mettler et al. 2001, van Halem et al. 2011), and often Mn

oxidation is omitted entirely from groundwater geochemical modeling (Thomas et al. 1994, Kübeck et al. 2009).

Nevertheless, the transient oxygen dynamics in well fields, especially bank filtration sites, suggest that the potential for *in situ* Mn oxidation exists, especially with low-Fe groundwater. This study tested whether water table fluctuations, similar in amplitude and frequency to those in a bank filtration site in Berlin, Germany (Massmann and Sültenfuß 2008), could supply enough dissolved oxygen (DO) to oxidize Mn. *Pseudomonas putida* GB-1, an obligate aerobe and well-studied Mn oxidizing bacterium, was selected to colonize a column of quartz sand with anoxic influent, subject to > 1 m water table fluctuations.

Experimental Section

Reagents

All chemicals used were reagent grade and used without further purification. All water used was 18 MΩ-cm deionized water (Barnstead, Nanopure). Solutions were stored in plastic containers that had been acid-washed in 5% hydrochloric acid. All nitric acid solutions were made with trace-metal-grade HNO_3 (Merck Suprapur, 65%).

Bacterial strain, media, and growth conditions

Pseudomonas putida strain GB-1 (generously provided by C. M. Hansel, Harvard University) was grown in Luria Broth (LB) at room temperature (23.2°C) from LB agar plates. In early stationary phase, cells were harvested by centrifugation (20 minutes at

4,000g) and resuspended in MSTG growth medium (Parikh and Chorover 2005) at pH

7.5: 2 mM $(NH_4)_2SO_4$, 0.25 mM $MgSO_4$, 0.4 mM $CaCl_2$, 0.15 mM KH_2PO_4, 0.25 mM

Na_2HPO_4, 10 mM HEPES, 0.01mM $FeCl_3$, 0.01 mM EDTA, 1 mM glucose, and 1 mlof

trace metal solution (10 mg l^{-1} $CuSO_4 \cdot 5H_2O$, 44 mg l^{-1} $ZnSO_4 \cdot 7H_2O$, 20 mg l^{-1}

$CoCl_2 \cdot 6H_2O$, and 13 mg l^{-1} $Na_2MoO_4 \cdot 2H_2O$). For Mn oxidation experiments, 0.1 mM

$MnCl_2$ was added to MSTG media. For the column study, 5-l batches of MSTG were

filter-sterilized (0.45 μm nitrocellulose, Whatman) and 1 mg l^{-1} NaBr was added to

alternate batches, which had no effect on cell growth or Mn oxidation capacity. Growth

of all bacteria was carried out with autoclaved or ethanol-rinsed materials under pure

culture conditions.

Reduction assays

To determine whether MSTG media and *P. putida* GB-1 were able to reduce Mn oxides,

3 batch experiments with hydrous Mn oxide-doped gels (Farnsworth and Hering 2010)

were conducted, with 3 replicates each. Because the microbial cells are physically

separated from the Mn oxide inside the gels, the assay could separately account for Mn

reduction inside the gel and Mn re-oxidation in solution, outside the gel. 25 ml MSTG

medium was added to sterile 50 ml centrifuge tubes. Two of the batches were inoculated

with 100 ml GB-1 from a dense ($OD_{600} \sim 1.0$) LB culture. At t=0, 3 hydrous Mn oxide-

doped gels each were added to the non-inoculated batch ("blank") and one of the

inoculated batches ("exponential"). All three batches were added to a rotary shaker at

180 rpm at room temperature. After the onset of stationary phase, at t=15 h, 3 hydrous

Mn oxide-doped gels were added to the second inoculated batch ("stationary"). At t=64

h, the gels were harvested and the solutions sampled. In both the gels and the solutions,

the remaining Mn was extracted first with 0.05 M $Cu(NO_3)_2$ in 0.05 M $Ca(NO_3)_2$, then

with 0.5% hydroxylamine-HCl to give an approximate measure of Mn(II) and total Mn

(Warden and Reisenauer 1991). Extracted solutions were filtered (0.2 μm nitrocellulose,

Whatman), diluted, and analyzed with ICP-MS (Agilent 7500cx). Solutions were also

monitored for OD_{600} at 15 and 64 h. Gel Mn data were analyzed using the MATLAB

code provided in the literature (Farnsworth et al. 2010) to estimate the pseudo-first-order

rate constants for Mn oxide reduction.

Oxidation assays

At the end of the column experiment, a series of batch experiments were used to compare

the oxidizing activity of the column effluent, the column influent, and the GB-1 culture

on agar plates at 4°C. 25 ml MSTG medium was added to sterile 50 ml centrifuge tubes.

Freshly prepared filter-sterilized medium was added to 4 tubes and degassed column

influent solution was added to a fifth tube. 15 μM $ZnCl_2$ and 100 μl column effluent

were added to one of the fresh MSTG batches. 100 μl of the column effluent were added

to a second fresh MSTG batch, and a third batch was inoculated directly from the GB-1

culture on a refrigerated agar plate. The fourth batch was not inoculated. After 34 h

shaken at 180 rpm at room temperature, samples were collected for $OD_{600.}$ Samples of

Mn(II) and total Mn (extracted as in reduction assays) were analyzed with ICP-MS.

Column design and flow conditions

Plastic flanges were glued to the ends of an 8-cm-inner-diameter, 1.5-m-length clear PVC

pipe (wall thickness: 5 mm). Removable plastic plates were affixed to the flanges with

screws, and sealed with a rubber O-ring between the plates and flanges. The influent and

effluent ports were through the plastic plates at top and bottom. In addition, the column

was fitted with three side ports (25, 50, and 75 cm from the column base) and a

ventilation valve 7.5 cm from the column top. PVC tubing (wall thickness: 2 mm)

connected the influent port to a 10-l reservoir and the effluent port to a 3-way splitter

open to the atmosphere. In downflow mode, water flowed by gravity into the column,

and the height of the splitter controlled the height of the water table inside the column

(Figure C.1).

Ten kg uniformly sized quartz sand (Fontaineblau, BDH Prolabo, 0.24 mm

average diameter) were slurry-packed in the column and held in place by a plastic mesh

(pore size 0.088 mm) lining the bottom plate. The sand filled 122 cm of the column with

a porosity of 0.39. The filled column was then flushed in upflow mode with 3.5 l of 5%

HCl, followed by > 50 l of 1 mM NaBr solution bubbled with N_2 (99.999%, < 2 ppm O_2)

to flush the acid and to remove the oxygen in the column; the side ports and ventilation

valve were closed. Once the effluent dissolved oxygen (DO) was < 10%, the column was

switched from upflow to downflow, and the influent solution was switched to N_2-sparged

MSTG without Mn. At this time, a 0.45 μm nitrocellulose filter membrane (Protran,

Whatman) was added between the top plate and the O-ring. The sand was inoculated

with 100 ml *P.putida* GB-1 culture (3.2×10^{11} cells l^{-1}) injected in the three ports and

added directly through the top of the column. The system was allowed to equilibrate with

no flow for 3 h, after which flow of N_2-sparged MSTG with Mn commenced (t = 0).

Flow through the column was maintained at an average of 3.2 ± 1.2 l d^{-1}, or

approximately one pore volume per day at the high water level. The visually observed

water level inside the column was lowered from approximately 135 cm to 32 cm after

30–50 h by decreasing the splitter height, then raised again after 30–50 h by restoring the splitter height (Figure C.1). The ventilation valve was open to allow air entry in the drained and refilled pore volume. Water table fluctuations with flow continued for 615 h; short flow interruptions (< 2 h) were required to degas fresh MSTG in the influent reservoir. Alternate batches of MSTG included 1 mg l^{-1} NaBr as a tracer to provide a qualitative assessment of the flow through the column over time. After 451 h (4 water table fluctuations), 15 µM $ZnCl_2$ was added to all subsequent influent solution.

The operation of the column was designed to minimize *P. putida* GB-1 taxis into the influent reservoir, as MSTG passed through a 0.45 µm filter and entered the column dropwise, mostly from the middle of the slightly sagging filter. Some MSTG, however, flowed intermittently along the column walls, and over 4 d, the bacteria were able to swim into the filter, most likely along these flow paths; Mn oxide and an opaque precipitate were observed along flow paths after 1 d of flow. Influent filters were therefore changed every 2–5 d when the clogged filters resulted in flow rates $< 2.2\ l\ d^{-1}$. The absence of DO in the influent solution inhibited significant microbial growth (i.e., no visually observable turbidity), but introduction of air to influent solution from the end of the experiment did yield cell growth (Table C.1).

Sampling and analyses

Samples were taken directly from the base of the column and from the collected effluent. Samples from the column base were analyzed for DO (polarographic DO probe, Thermo Electric) and pH (Ross Sure-Flow, Thermo Electric), and the volume of the collected effluent was volumetrically estimated to calculate the average flow rate. Filtered (0.2 µm cellulose acetate, VWR) and unfiltered subsamples of all effluent samples were diluted

$100\times$ with 1% HNO_3 for ICP-MS (Agilent 7500cx). The DO probe was calibrated before each sample; the pH electrode was calibrated daily.

At the end of the column experiment, the column was drained and frozen for 3 days. It was then thawed and the sand removed with a plastic core tube. Vertical sections of the sand (from the top of the column: 2×3.5 cm, 2.5 cm, and 9×12.5 cm in length) and one sample of unused sand were freeze-dried and milled for 90 s at 30 Hz with a ZrO_2 milling set (< 50 μm grain size, Retsch MM400), then pressed into 32 mm pellets for XRF analysis (Spectro XEPOS). A subsample (180 mg) from the top section was thoroughly mixed with 20 mg of wax and pressed into a pellet (diameter: 1.3 cm) for analysis by Mn K-edge X-ray absorption near edge structure (XANES) and extended X-ray absorption fine structure (EXAFS) spectroscopy. Spectra were measured at the XAS beamline at the Angströmquelle Karlsruhe (ANKA, Karlsruhe, Germany). The Si(111) monochromator was calibrated by setting the first inflection point of the absorption edge of a Mn metal foil to 6539 eV. The sand pellet was measured at room temperature in fluorescence mode using a 5-element Ge solid state detector. Spectral data processing and linear combination fitting (LCF) were performed using the software code Athena (Ravel and Newville, 2005). The XANES spectrum was evaluated from 6530 to 6640 eV; the EXAFS spectrum from 2 to 10 Å^{-1} (k-range relative to E_0 of 6550 eV). Reference spectra for LCF included aqueous Mn^{2+} (100 mM $Mn(NO_3)_2$; measured at SUL-X beamline at ANKA), δ-MnO_2 and hexagonal birnessite (phyllomanganate reference spectra from literature (Webb et al. 2005), kindly provided by Sam Webb, SSRL).

Data analysis

Hydraulic conductivity during the experiment was calculated with the Darcy equation:

$$K = v_D \frac{L}{\Delta H} \tag{5-1}$$

where K is the hydraulic conductivity, v_D is the Darcy velocity equal to the volumetric

flow rate divided by the cross-sectional area, L is the column length, and ΔH is the head

difference between the column water level and the effluent splitter. The dispersion

coefficient of the column was estimated from Br breakthrough with pulsed inlet

concentration (Figure C.2). Smooth breakthrough curves at constant water levels (i.e., 0–

48 h, 190–234 h, 239–270 h, 326–358 h, and 560–592 h) were modeled in CXTFIT

(Toride et al. 1995) to solve for the dispersion coefficient, D. Pseudo-first-order Mn

removal rates were estimated from the 1-D advective-dispersive transport equation:

$$\frac{\partial C}{\partial t} = D \frac{\partial^2 C}{\partial x^2} - \frac{v_D}{\varphi} \frac{\partial C}{\partial x} - kC \tag{5-2}$$

where C is the dissolved Mn(II) concentration, D is the dispersion coefficient, φ is the

porosity, and k is a pseudo-first-order removal rate. Solving for local minima in C(t),

with a Peclet number $\gg 1$ (advection dominates dispersion), this equation simplifies to:

$$\frac{\partial C}{\partial t} = - \frac{v_D}{\varphi} \frac{\partial C}{\partial x} - kC = 0 \ . \tag{5-3}$$

Integration over the column length yields the following expression for k:

$$k = - \frac{v_D}{\varphi \cdot L} \ln \frac{C}{C_0} \tag{5-4}$$

where C/C_0 is the value at the local minimum. Damköhler numbers, which assess the

ratio of a reactive flux to advective flux, were calculated with this expression (Battersby

et al. 2006):

$$Da = \frac{k \cdot C \cdot V}{Q \cdot C} \tag{5-5}$$

where k is the pseudo-first-order rate coefficient [h^{-1}], V is the column volume [l], and Q is the volumetric flow rate [$l\ h^{-1}$]; the Mn concentration, C, cancels out from the top and bottom of equation (5-5). For Da > 3, a reaction can be assumed to reach completion.

Results and Discussion

Water table fluctuations and dissolved oxygen

Over 615 h, the water table inside the column was oscillated 6 times from a high water level to a water level approximately 1.3 m lower and back to the high water level (Figure 5.1a); for clarity of description, one "fluctuation" or "oscillation" refers to a complete high-low-high water table cycle. The level of wetted sand was visually estimated to be ~ 32 cm above the column base, but the actual water table was calculated to be < 5 cm based on the hydraulic conductivity of the column (calculated at the high water level). For sand with a 0.22 mm grain diameter and a porosity of 0.39, a 30 cm capillary fringe height is reasonable (Lohman 1972). The hydraulic conductivity varied between 0.005 and 0.017 cm s^{-1} with no significant trend during column operation.

Air entered the unsaturated pore spaces when the water table was low, and was potentially entrapped when the water table was raised. The anoxic column influent acquired DO as the solution percolated downward through the unsaturated sand (maximum effluent DO of 3.6 mg l^{-1} = 42% saturation at 23.2°C), but did not acquire significant amounts of DO (< 1 mg l^{-1}) when the water table was high. Effluent DO levels are "net" DO concentrations, which reflect oxygen mass transfer from the gaseous phase to the dissolved phase as well as DO consumption by microbial respiration; the

actual dissolved oxygen delivered to the aqueous phase is unknown. Some early

problems with leaks through the side ports, as seen in the sharp drop in water level

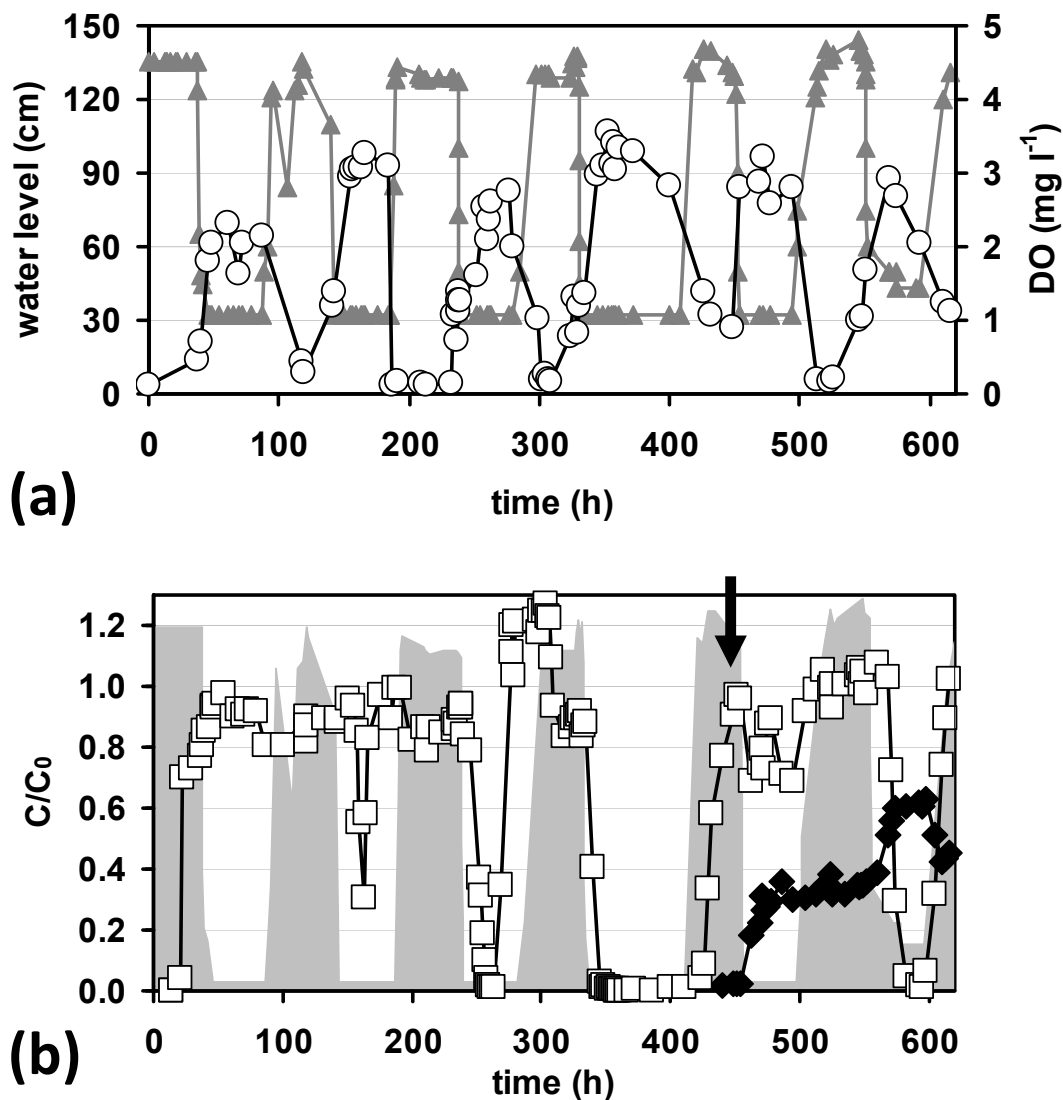around 100 h, did not significantly affect DO dynamics.

(a)

(b)

Figure 5.1. (a) Changes in the visible water level in the column (▲) and the effluent dissolved oxygen (○) over time. (b) Filtered relative effluent concentrations of Mn (□, $C_0 = 100\ \mu M$) and Zn (◆, $C_0 = 15\ \mu M$). The arrow denotes the addition of 15 μM Zn to the influent. For reference, the water level in the column is shown in the shaded profile (note the vertical scale is different than (a)). The residence time of the column was approximately 16.3 h.

Manganese removal and filter ripening

After Mn uptake in the column in the first 1–2 pore volumes of influent (t < 30 h), Mn

removal from the column influent coincides with lower water levels, beginning 42 h after

the first water table decrease (Figure 5.1b). The onset of Mn removal occurs 16, 8, and 4

h after the subsequent water level decreases (Table 5.1). The duration of the Mn removal

also increases with 3 subsequent water level fluctuations, from approximately 14 h to 76

h in the fourth oscillation. Furthermore, the Mn removal increased to > 99% by the third

oscillation. Estimated pseudo-first-order rate constants also increase with the first 4

oscillations (see further rate discussion below). These parameters are all indicative of

"filter ripening" processes, which are typical in water and wastewater treatment sand

filters (Frischherz et al. 1985, Mouchet 1992). Two regions of Mn washout (C/C$_0$ > 1) at

280 h and 513 h are likely a release of adsorbed Mn(II) in the column after a 10%

decrease in influent Mn concentration due to inter-batch heterogeneity of MSTG medium.

Table 5.1. Mn removal parameters for each water table oscillation

oscillation	lag phase (h)	duration of removal (h)	minimum C/C$_0$	pore velocity cm h^{-1})	k (h^{-1})	Da[a]
1	42	14	0.804	7.2	0.01	0.22
2	16	10	0.309	6.1	0.06	1.2
3	8	24	0.009	6.2	0.24	4.7
4	4	76	0.002	7.3	0.37	6.2
5[b]	28	17	0.688	7.5	0.02	0.41
6	19	29	0.011	6.5	0.24	4.5

[a] Damköhler number, the ratio of reactive flux to advective flux
[b] 15 μM ZnCl$_2$ was added to the influent at the beginning of this oscillation.

As low water levels enhanced oxygen delivery to the aqueous phase, Mn removal at low

water levels is consistent with Mn oxidation. Elevated DO was present in the effluent

during the periods of greatest Mn removal. This is expected, since the column was

colonized with *P. putida* GB-1, an obligate aerobe whose ability to oxidize Mn is oxygen-dependent (Okazaki et al. 1997). In batch studies, *P. putida* GB-1 commences Mn oxidation at the end of exponential phase, approximately 12 h after inoculation in MTSG at 30°C (Parikh and Chorover 2005). Orange-brown precipitates were visible on the sand at the top of the column after 44 h, and with subsequent water table fluctuations, they increased in spatial extent. XAS with linear combination fitting analysis further confirmed that the Mn in the topmost part of the column at the end of the experiment was Mn(IV) oxide (spectral combination of hexagonal birnessite and δ-MnO$_2$) with ca. 20% adsorbed Mn(II) (Figure C.3, Table C.2). XAS studies suggest *P. putida* MnB1, which is closely related to GB-1, and *Bacillus* sp. SG-1 produce similar Mn oxides (Villalobos et al. 2003, Webb et al. 2005). Therefore, filter ripening processes for Mn removal may be related to the development of an active zone of Mn oxidation.

Microbial biofilm growth and physiological adaptation to the column conditions likely contribute to the filter ripening, or enhanced Mn removal over time. Common in groundwater (DePalma 1993) and closely related to a strain isolated from Mn-oxide encrustations on water pipes (MnB1) (Caspi et al. 1998), *P. putida* GB-1 forms biofilms attached to negatively charged surfaces (like silicates). Mn oxidation subsequent to attachment does not interfere with adhesion (Parikh and Chorover 2005), although it does result in a Mn oxide coating of the cell walls; complete coating of actively oxidizing microbial surfaces may account for the sharp increases in effluent Mn during filter ripening. Based on the appearance of planktonic cells (and in some cases, biofilm and Mn oxides) in the column effluent, the initial inoculation of *P. putida* GB-1 quickly (< 60 h) spread through the sand column. The absence of biofilm and Mn oxides observed in

the collected effluent after three water table fluctuations suggests that the biofilm in the column became less susceptible to washout over time. *P. putida* mt-2, a weak Mn oxidizer related to GB-1 (Francis and Tebo 2001), survived 24 h periods of anoxia in batch experiments by up- and down-regulating gene expression based upon DO availability (Martinez-Lavanchy et al. 2010), further suggesting microbial adjustment to the column conditions was a critical component of filter ripening.

The addition of 15 μM Zn at the beginning of the fifth water table oscillation (451 h) interfered with the Mn removal process (only 31% removal). Although already present in MSTG at a low concentration (150 nM), 15 μM Zn in the medium inhibited microbial Mn oxidation; cell growth was slightly enhanced (Table C.1). The lag phase for removal increased from 4 h to 28 h, and the duration of removal decreased from 76 h to 17 h (Table 5.1). Nevertheless, 99% Mn removal was restored within one water table oscillation, with a lag phase of 19 h and a 29 h duration of removal. The estimated pseudo-first-order rate constant similarly recovered to that of oscillation 3 (0.24 h^{-1}), all despite the continued presence of Zn.

The Mn and Zn content in the column solids at the end of the experiment (Figure 5.2) lead to one possible mechanism of microbial adjustment to the presence of Zn: the physical separation of Zn removal and Mn removal zones. The Mn concentration had a steep gradient from 210 mg kg^{-1} at the top of the column to 9 mg kg^{-1} in the 63–75 cm section, for an accumulation zone of approximately 60 cm. Mn was above the 6 mg kg^{-1} sand background throughout the profile, and the total Mn accumulation (XRF data, 2.42 mmol) was in excellent agreement with the total Mn removal from solution ($C/C_0 \times Q$, 2.46 mmol). Zn also had a steep gradient from 8 mg kg^{-1} at the top of the column to < 2

mg kg^{-1} in the 100–113 cm section, for an accumulation zone of approximately 22 cm. Below the accumulation zone, Zn was ≤ 1.5 mg kg^{-1}, the sand background. Zn accumulation (48 μmol) was in acceptable agreement with the total Zn removal from solution (93 μmol), considering that the Zn data approached the XRF practical quantitation limit (~ 1 mg kg^{-1}) and that the initial flush of acid through the column may have resulted in lower initial Zn in the column than measured in the unused (background) sand. A steep gradient in solid-phase P, perhaps indicative of biofilm, was also measured (Figure C.4), whereas Br was constant with depth (not shown, 0.3 mg kg^{-1}). Thus, it is possible that Zn was adsorbed to older Mn oxides or biofilm material in the first cm of sand, then new Mn was oxidized below this zone. Micro-scale zonation is also possible. The lack of Zn breakthrough (maximum C/C$_0$ = 0.63, Figure 5.1b) suggests the combined sorption capacity of the sand, Mn oxide, and biofilm was not reached.
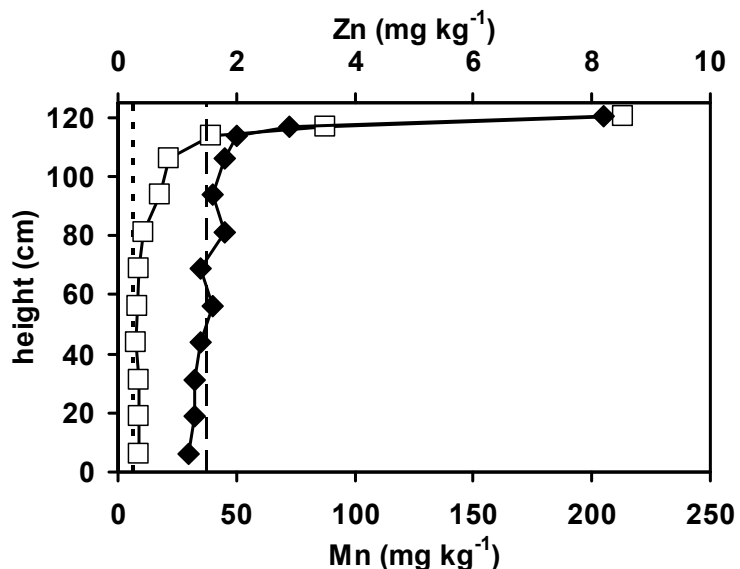

Figure 5.2. XRF profile of Mn (□) and Zn (◆) along the column at the end of the experiment. Dashed lines indicate the background Mn (short dashes) and Zn (long dashes) of unused sand. The plotted height is the average of the vertical section.

Rates of Mn removal

Mn removal rates were estimated with 1-D advective-dispersive transport and a pseudo-first-order sink term. The dispersion coefficient in the column was between 1 and 7 cm^2 h^{-1}, which corresponded to Peclet numbers between 120 and 700. For Pe $\gg$ 1, the dispersion term in the transport equation could be omitted. For the minima in C vs. t $\left(\frac{\partial C}{\partial t} = 0 \right)$, pseudo-first-order Mn removal rates then depended only on $C/C_{0, min}$, the length of the column, and the pore velocity (Table 5.1). These rates serve merely as a lower bound for the rate constant responsible for the decrease in C/C_0, since only for oscillation 4 was steady state clearly reached (Figure 5.1b). Furthermore, the minimum measurable value of C/C_0 was 0.001, based on the practical quantitation limit of the ICP-MS (0.9 nM) and 100-fold sample dilution. The Damköhler numbers for these rates ranged from 0.2 to 6.2, which suggests that for low rates in oscillations 1, 2, and 5, the advective flux prevented the removal reaction from reaching completion. Otherwise, the rates in the column were not limited by flow conditions.

Manganese removal in the column is a net effect of multiple processes including abiotic reduction and oxidation by the microbial medium, microbial oxidation and reduction, and oxide-catalyzed oxidation. Photoreduction of Mn is assumed to be insignificant in the sand column (Xyla et al. 1992). Mn adsorption to oxide surfaces has a reported (Davies and Morgan 1989) half-life of 5 min, which is insignificant on the multi-hour time scales of Mn removal; sorption to biofilm components is assumed to be similarly rapid. Mn-oxide-doped gels were used to assess the ability of the microbial medium and *P. putida* GB-1 to reduce Mn. Pseudo-first-order rate constants were 0.003

h^{-1} and 0.005 h^{-1} for the medium alone and the medium with cells, respectively (Table C.3). These rate constants are in the range of O_2- and nitrate-reducing sediments (< 8 cm depth) in a German lake, measured with the same gel technique (Farnsworth et al. 2010). Oxidation by the microbial medium was insignificant (Figure C.5).

Below pH 9, abiotic oxidation rates are generally slow compared to microbial oxidation rates (Morgan 2005). The effluent pH varied between 6.35 and 7.55, despite a constant influent pH of 7.5 (Figure C.6), which further suggests that abiotic oxidation rates were irrelevant. Estimates of homogeneous (Morgan 2005) and surface-catalyzed (by both quartz sand (Davies and Morgan 1989) and Mn oxide (Morgan 2000)) Mn oxidation at pH 7 with full oxygen saturation indicate that abiotic oxidation is a minor contribution to the observed net oxidation rates (Table 5.2). Despite a large quantity of sand available to oxidize Mn, its low surface area (0.01 m^2 g^{-1} estimated for spherical grains) and low adsorption of Mn(II) at circumneutral pH result in a rate 3 orders of magnitude lower than the lowest observed rate. Further details on the rate calculations are available in Appendix C.

Thus the net observed oxidation rates (1–37 μM h^{-1}) are assumed to derive almost entirely from microbial oxidation. Although not directly confirmed at the end of the experiment, *P. putida* GB-1 is assumed to be the only microorganism in the column (Table C.1). In shaken containers with dense (ca. 10^{12} cells l^{-1}) cultures, *P. putida* GB-1 has been shown (Okazaki et al. 1997) to oxidize Mn as fast as 240 μM h^{-1}. *Leptothrix discophora* SS1, another common Mn-oxidizing aerobe, oxidized Mn at rates up to 390 μM h^{-1} under the same batch conditions (Boogerd and de Vrind 1987). That these rates were measured in undefined Lept medium, which contains 0.5 g l^{-1} each of yeast extract

and Casamino acids, accounts for some enhancement relative to the observed rates in
defined minimal MSTG medium.

Table 5.2. Potential rates of Mn oxidation and reduction in the column

oxidation	homogeneous (Morgan 2005)	2×10^{-5} μM h^{-1}
	SiO$_2$-catalyzed (Davies and Morgan 1989)	2×10^{-3} μM h^{-1} [a]
	Mn oxide-catalyzed (Morgan 2000)	0.03 μM h^{-1} [b]
	P. putida GB-1 (Okazaki et al. 1997)	240 μM h^{-1} [c]
	Leptothrix discophora SS1 (Boogerd and de Vrind 1987)	390 μM h^{-1} [c]
reduction	MSTG	0.3 μM h^{-1}
	MSTG + *P. putida* GB-1	0.5 μM h^{-1}
net observed oxidation rate	oscillation 1 (minimum)	1 μM h^{-1}
	oscillation 4 (maximum)	37 μM h^{-1}

[a] Rate assumes oxidation occurs throughout the column with 100% DO saturation.
[b] Rate uses the average final solid phase Mn (20 mg kg^{-1}) throughout the column with 100% DO saturation.
[c] Rate measured for ca. 10^{12} cells l^{-1} in Lept medium (Boogerd and de Vrind 1987) with 100% DO saturation

Two additional factors that contribute to the slower measured rates are the pH and
dissolved oxygen. General bacterial cell physiology may lead to the accumulation under
anaerobic conditions of metabolites, which can then deliver protons upon reintroduction
of oxygen (Balcke et al. 2004). The general inverse trend of pH and DO (Figures 5.1a
and C6) suggests this may be the case. For *L. discophora* SS1, the maximum oxidation
rate occurs at pH 7.5, with a steep decline to 30% of the maximum rate (Zhang et al.
2002) or no oxidation at all (Boogerd and de Vrind 1987) at pH 6.5. On the other hand,
pH decreases were observed during both growth of *L. discophora* and Mn oxidation (the
latter is predicted from stoichiometry as well) (Boogerd and de Vrind 1987), so it is
difficult to assess if the observed pH dynamics are merely a by-product of microbial

growth and oxidation in the top cm of the column or if they actively limited a large portion of the microbial community.

Experiments with varying delivery rates of DO to GB-1 batch cultures revealed a strong dependence of Mn oxidation rate on the measured DO in late logarithmic phase (Okazaki et al. 1997). Although its growth was unaffected by DO concentrations between 10–25% saturation (20°C), Mn oxidation required DO > 14% in late logarithmic phase. The DO concentrations in that study reflect a balance between the delivery rates (enhanced by variable shaking speed) and microbial consumption, not an absolute cutoff in oxygen concentration for Mn oxidation; even under rigorous shaking, the DO concentration in early- to mid-logarithmic phase was nearly zero (Okazaki et al. 1997). Generally, in the presence of oxygen-consuming processes, oxygen mass transfer across the air-water interface is enhanced (Haberer et al. 2011); this is expected in the column as well. Interestingly, the maximum oxidation rate in early stationary phase corresponded with a DO of approximately 27% saturation (2.5 mg l^{-1}) (Okazaki et al. 1997), which is similar to the highest measured DO in the column effluent (3.6 mg l^{-1}). Literature studies of *P. putida* species that aerobically biodegrade organics similarly show decreasing degradation rates proportional to DO exhaustion, which rapidly recover upon reintroduction of oxygen (Balcke et al. 2004, Bauer et al. 2009, Martinez-Lavanchy et al. 2010). Thus, the fluctuation of DO levels in the column between < 1 mg l^{-1} and 3.6 mg l^{-1} (maximum) inhibited the microbial Mn oxidation rate, relative to those measured in fully oxygenated batches.

Implications for groundwater systems

The downflow setup, necessary to prevent *P. putida* taxis into the influent solution, limited the amount of air entrapment possible. This arrangement is more similar to rain percolation than to water table fluctuations in the field, for which rising water levels are expected to derive from lateral or upward water flux. Although the Peclet number and the frequency and amplitude of the water table fluctuations (Massmann and Sültenfuß 2008) were chosen to be representative of bank filtration sites in Berlin, Germany, the microbial medium and microbial community are not representative of field conditions. High amounts of phosphate (0.4 mM) and organic carbon (180 mg l^{-1} glucose) are unlikely in uncontaminated shallow aquifers; even numerical dominance of *P. putida* species in soils generally means < 14% of culturable microbes (DePalma 1993). The purpose of this study, however, was to test whether the DO supplied by water table fluctuations is sufficient for Mn oxidation. Complete removal of 100 μM Mn(II) was indeed possible with the supplied DO; this Mn concentration is ten times higher than groundwater Mn concentrations considered to be problematic (or at least, which require treatment post-extraction) in Berlin (Massmann et al. 2008b) and Fredericton, Canada (Thomas et al. 1994). In general, Mn oxidation and transient DO concentrations are largely ignored in groundwater geochemical modeling (Thomas et al. 1994, Kübeck et al. 2009), but this study suggests that Mn oxidation in shallow groundwater could be more relevant than previously thought.

Key aspects that could affect the presence of a Mn oxidation zone in shallow groundwater include the source of the Mn(II), the depth of DO penetration, the depth of microbial Mn-oxidizing activity, and the amount of time for the microbial community to

adjust to the available Mn. Vertical zonation of bank filtrate has been previously observed (Massmann et al. 2008b), and if the Mn(II) is present below the depth of DO penetration and/or microbial Mn-oxidizing activity, very little *in situ* Mn oxidation potential exists. Microbial communities in sand filters for Mn removal require a notoriously long time ($\geq$ 8 weeks) for startup (Frischherz et al. 1985, Mouchet 1992), and Fe^{2+} and ammonium interfere with Mn-oxidation (Frischherz et al. 1985, Katsoyiannis and Zouboulis 2004, de Vet et al. 2010). Even under ideal conditions, water treatment processes may still provide greater efficiency and faster rates than *in situ* Mn oxidation; removal rates in this study were 100$\times$ slower than those for aerated groundwater treatment columns with beads coated in Mn oxides and a mixed *Gallionella* and *Leptothrix* biofilm community (1044 μM h^{-1}) (Katsoyiannis and Zouboulis 2004). Furthermore, massive microbial growth and Mn oxide formation in the aquifer could lead to clogging, although no significant change in hydraulic conductivity was observed in this study. Nevertheless, engineering studies with longer time horizons and larger-amplitude and less frequent water table oscillations, which would deliver more oxygen to the shallow groundwater, could perhaps optimize the *in situ* oxidation process to provide intransient Mn removal.

Acknowledgements